Sensitivity enhancement of fiber-optic refractive index sensor based on multimode interference with gold nanoparticles



2015 Jpn. J. Appl. Phys. 54 04DL07

(http://iopscience.iop.org/1347-4065/54/4S/04DL07)

Japanese Journal of Applied Physics **54**, 04DL07 (2015) **REGULAR PAPER**
http://dx.doi.org/10.7567/JJAP.54.04DL07

# Sensitivity enhancement of fiber-optic refractive index sensor based on multimode interference with gold nanoparticles

Shuji Taue*, Hiroyuki Daitoh, and Hideki Fukano

*Graduate School of Natural Science and Technology, Okayama University, Okayama 700-8530, Japan*
E-mail: taue@okayama-u.ac.jp

Received September 11, 2014; accepted January 22, 2015; published online March 25, 2015

In this study, we investigated combinations of fiber-based multimode interference (MMI) sensors with gold nanoparticles (NPs). Gold NPs were synthesized and attached to the MMI sensor region using a silane-coupling agent. Light absorption due to the NPs was confirmed at wavelengths of 560 nm and longer, including the telecommunication band (1300–1600 nm). We examined the variation in the interfered wavelengths with changes in the medium surrounding the MMI sensor, both with and without NPs. The interfered wavelengths were redshifted when the refractive index (RI) increased, and the shift with NPs was almost twice as large as the shift without NPs. We determined the sensitivity of the MMI sensor with NPs to be approximately 218.28 nm/RIU (refractive index unit) in a refractive index range from 1.31535 to 1.35199.


## 1. Introduction

Evanescent waves on the surface of an optical fiber can be used to measure the absorption,[1–4] refractive index (RI),[5–13] and temperature[14,15] of the surrounding material. Owing to the rapid proliferation of optical fiber telecommunications systems, the quality of these systems has increased while the cost has decreased. Optical fibers in sensors have attracted attention because of their compact size, high sensitivity, ease of fabrication, and portability. Furthermore, optical fiber sensors are not affected by electro-magnetic noise, and silica fibers are stable in many chemical environments. One attractive structure for sensitive measurement is a multimode interference (MMI) structure,[10–15] which employs the optical interference between modes in an unclad multimode fiber (MMF). The MMI sensor can detect RI changes around the fiber very precisely as changes in its interference spectrum.

Many RI sensors incorporating the fiber sensor that uses the localized surface plasmon resonance (LSPR) of noble-metal nanoparticles (NPs) have been reported, where NPs are attached to the sensor surface. In particular, gold NPs are used for biosensing applications because of their good biocompatibility and sensitivity.[16] These sensors detect the resonant characteristics changes in the visible wavelength range, when the RI around the nanoparticle varies.[17–19] The resonance wavelengths are not restricted to the visible range and also appear in the near-infrared range, including the telecommunication band. The wavelength range of the LSPR depends on the nanoparticle size and shape and the degree of aggregation. The aggregated NPs are important for surface-enhanced Raman scattering (SERS) because of strong inhomogeneity of the electric field along coupled NPs.[20] It is known that fully aggregated NPs cause higher electric field enhancement at longer wavelengths owing to the dipole–dipole interaction of aggregated NPs.[21] A signal enhancement of an immune sensor has been reported using gold NPs conjugated on recognition proteins.[22] The effective RI change due to NPs enhances the interference spectral shift.

In this study, we synthesized gold NPs and attached them to the surface of the fabricated MMI sensor region. This configuration is useful for biosensing applications because of its disposability and the excellent biocompatibility of both gold and silica. Because of its simple and fine shape, the sensor will be employed within a microfluidic device or living tissues in the future. The MMI sensor can detect the effective RI change due to the electrooptic effect caused by the electric field enhancement with NPs as changes in its interference spectrum. The sensitivity of the MMI sensor was evaluated by measuring transmission spectra while changing the RI of the surrounding medium.[23] The effective RI was measured, and the sensitivity improvement was confirmed by the experimentally obtained wavelength shifts for RI transitions.

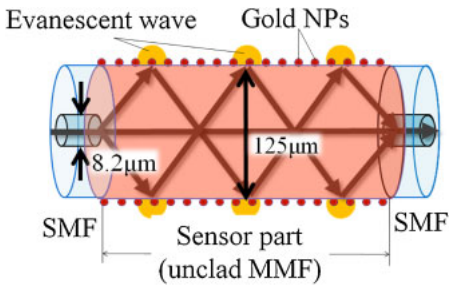


**Fig. 1.** (Color online) MMI structure with gold NPs.

## 2. Operation principle of multimode interference with gold NPs

Planar multimode waveguides produce periodic focusing points in a phenomenon known as MMI.[24] The optical fiber MMI follows the same principles as those of a cylindrical waveguide. The unclad MMF is sandwiched between two single-mode fibers (SMFs) as input and output fibers. As shown in Fig. 1, the gold NPs are attached to the MMF surface. The light from the input fiber is diffracted and split into propagation modes in the MMF. The LSPR of the attached NPs is excited by the evanescent wave generated by total reflection of the multimode light. The resonant wavelength of the LSPR depends on the RI of the surrounding medium, the nanoparticle size and shape, and the distance between particles, among other factors. In this study, the amount of absorption due to LSPR in the telecom wavelength range was controlled by altering the synthesis conditions to change the size and aggregation of NPs. The light coupled into the output fiber is interfered as a result of the modal

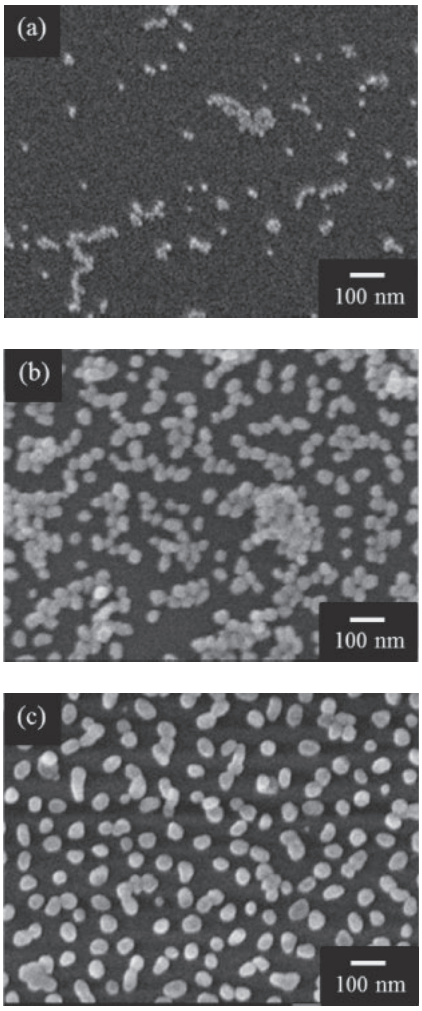


**Fig. 2.** SEM images of gold NPs synthesized from three types of solutions with trisodium citrate added in concentrations of (a) 0.4%, (b) 0.07%, and (c) 0.03% (w/v) to 0.01% (w/v) hydrogen tetrachloroaurate(III) tetrahydrate solutions.

dispersion. The interfered spectrum obtained from the output light through the MMI structure is affected by the surrounding medium of the MMF. Because the surrounding medium of the MMF acts as a cladding layer, variation in the RI including those of NPs induces a Goos–Hänchen shift (optical phase shift)[25] in the total reflection region, resulting in a change in the interference signal.

## 3. Experimental methods

We used a 125-μm-diameter, 80-mm-long unclad MMF of pure silica sandwiched between SMFs with a core diameter of 8.2 μm, which serve as input and output fibers. Each fiber end was connected to a white light source or an amplified spontaneous emission light source and an optical spectrum analyzer to evaluate optical interference in the spectral domain.

Gold NPs were synthesized through the reduction of hydrogen tetrachloroaurate(III) tetrahydrate ($HAuCl_4 \cdot 4H_2O$) using trisodium citrate ($C_6H_5O_7Na_3$).[26] To control the size and the dispersion of NPs, we synthesized three types of gold NP solutions by adding the trisodium citrate in concentrations of (a) 0.4%, (b) 0.07%, and (c) 0.03% (w/v) to 0.01% (w/v) hydrogen tetrachloroaurate(III) tetrahydrate solutions. The trisodium citrate was also used to protect the NPs. Figure 2

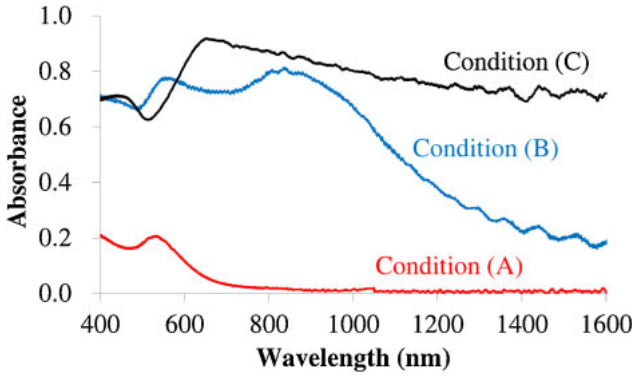


**Fig. 3.** (Color online) Absorption spectra of three types of gold NPs attached to the hetero-core fiber structure.

shows SEM images of NPs synthesized with the three conditions mentioned above. From the images, the averaged diameters of synthesized NPs were 15, 37, and 53 nm for concentrations (a), (b), and (c), respectively. The NPs were attached to the MMF using a 1% (v/v) aqueous solution of 3-aminopropyltriethoxysilane (APTES) as a silane-coupling agent.[27] The attachment conditions using NPs with concentrations (a), (b), and (c) are indicated as (A), (B), and (C), respectively. Figure 3 shows absorption spectra of the three cases of gold NPs attached by the same procedure to a hetero-core fiber structure.[28] The output signal from the hetero-core fiber structure represents only the absorbance spectrum without interference. In the case of attachment condition (A), only the characteristic absorption occurred at around a wavelength of 550 nm. On the other hand, absorbance with a broadened band at longer wavelengths, including telecommunication wavelengths, occurred under conditions (B) and (C). From these absorption spectra, the size and degree of aggregations of NPs attached to the MMF were responsible for the absorption spectral shapes. The absorbance with a broad and longer wavelength spectrum is caused by the larger size or closely deposited NPs resulting from aggregation.[21] It was considered that the electron gas in aggregated NPs was excited at telecommunication wavelengths, and it was considered to affect the effective RI.

## 4. Results and discussion

The transmission spectral shift due to the varying RI of the surrounding medium was observed using an amplified spontaneous emission light source with a wavelength range of 1520–1620 nm. Figure 4 shows the measured transmission spectra of the MMI sensor with NPs of conditions (A), (B), and (C) and without NPs when the material around the sensor region was either water or ethanol. The wavelength shift caused by the RI change around the fiber was measured from the spectral dip observed at around 1540 or 1550 nm, as denoted by an arrow. The interference patterns composed of peaks and dips were nearly unchanged. The wavelength shift was varied by the adhesion of NPs. In particular, the gold NPs of conditions (B) and (C) attached to the MMF led to a clear increase in the wavelength shift, although a slight decrease in transmission intensity and broader and more gradual interference dip signals were observed because of the light scattered by the NPs.[29] Figure 5 shows the wavelength shift for the varying RI during the transition from water to

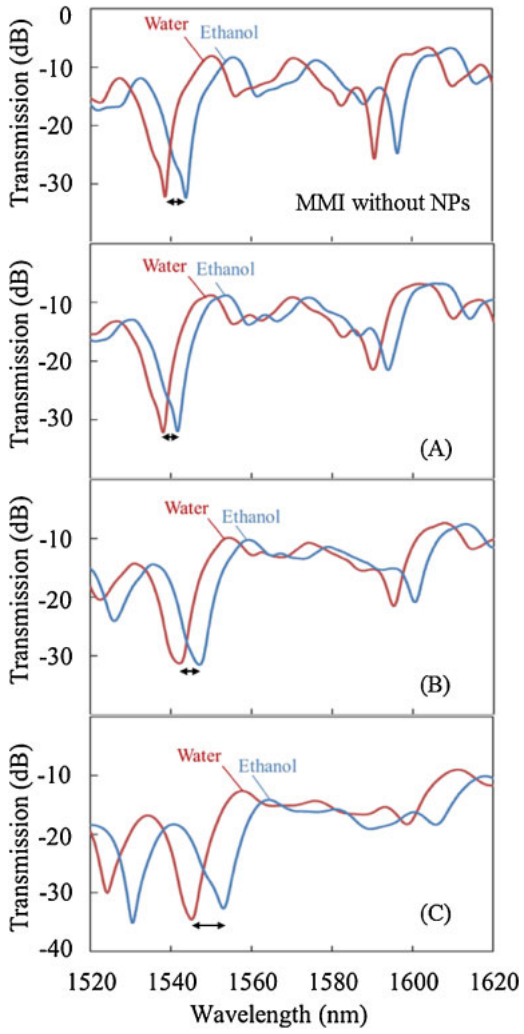


**Fig. 4.** (Color online) Transmission spectra of the MMI without NPs and MMI with NPs of conditions (A), (B), and (C), when the material around the sensor region was either water or ethanol.

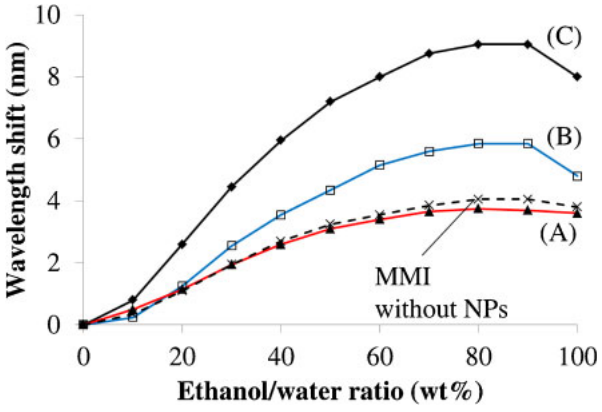


**Fig. 5.** (Color online) Ethanol/water ratio versus dip signal wavelength shift obtained using the MMI structure with three conditions of NPs and without NPs.

ethanol, as measured from the MMI structures with three different conditions of NPs as well as without NPs. The wavelength shifts for all of the MMI structures have the same characteristic peak at 80 to 90% of the ethanol/water ratio. This trend corresponds to the reported tendency of RI. The results for the MMI with NPs of condition (A) and without

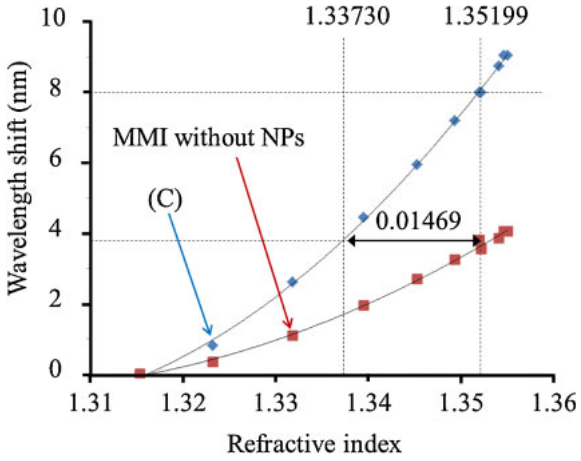


**Fig. 6.** (Color online) RI transitions versus wavelength shifts for MMI without NPs (red squares) and with NPs of condition (C) (blue diamonds).

NPs are similar, but the MMI sensors with NPs of conditions (B) and (C) show a larger shift. The wavelength shifts due to the change from water to ethanol are 3.75 and 8.00 nm for the MMI sensors without NPs and with NPs of condition (C), respectively. As shown in Fig. 3, the wavelength shift for each type of NPs attached to the sensor region appeared to correspond to the amount of absorption in the wavelength range of 1400–1600 nm. As previously described, the optical phase shift in the total internal reflection region causes the interference signal to shift. The enhancement of this shift definitively indicates that the optical phase shift increase is related to the size and the adhesion state of the NPs at the interface. A larger number and size of NP aggregates on the MMF lead to larger change in the effective RI and enhances the interference spectral shift.[22)]

In order to determine the relationship between the wavelength shift and RI, we referred to the reported value of the RI for the volume ratio of ethanol in water.[30)] The obtained sensitivities of the MMI sensors with NPs of conditions (A), (B), and (C), and without NPs were approximately 98.23, 130.97, 218.28, and 102.32 nm/RIU, respectively, with an RI range from 1.31535 (water) to 1.35199 (ethanol). The sensitivity of the MMI RI sensor was roughly twice as high when using gold NPs of condition (C) as compared with the case without NPs. To consider the sensitivity enhancement due to the presence of gold NPs, we estimated an effective RI value including those of the NPs. Figure 6 shows the experimentally obtained wavelength shifts with the RI of water as a reference. Red squares and blue diamonds indicate results for the MMI without NPs and with NPs of condition (C), respectively. Fitted curves for each plot are also represented in the figure. The wavelength shift of 3.8 nm for the RI of 1.35199 obtained from the MMI sensor without NPs corresponds to the RI of 1.33730 for the MMI sensor with NPs of condition (C). This consideration indicates the effective RI enhancement of 0.01469 due to the presence of gold NPs. The effective RI enhancement was thought to result from the electrooptic effect caused by electric field enhancement at the aggregated NPs. The increased effective RI led to the improvement in the sensitivity, as shown in Fig. 6. As a result, approximately twofold higher sensitivity was achieved by the attachment of the gold NPs.

## 5. Conclusions

In this study, we investigated combinations of MMI sensor and gold NPs. The amount of extinction in the telecommunication band was controlled by changing the concentration of the trisodium citrate used as a reduction agent and disperser. By using MMI with NPs, transmission decreased and the spectra became more gradual, but the spectral shift increased with the varying RI of the surrounding medium. The MMI shift with NPs of condition (C) was almost twice as large as that for only the MMI. From the results, it is considered that the increase in the spectral shift is related to the amount of extinction in the telecommunication band. The resultant sensitivity of the MMI sensor with NPs was approximately 218.28 nm/RIU for a RI range from 1.31535 to 1.35199 in the telecommunication band. The sensitivity of the RI sensor using the MMI structure could be easily improved by accurately controlling the adhesion of the gold NPs. Furthermore, this sensor system has potential in biosensing applications because both gold NPs and silica optical fibers have good biocompatibility.

## Acknowledgement

This work was supported by JSPS KAKENHI Grant Number 24656257.

1) P. H. Paul and G. Kychakoff, Appl. Phys. Lett. **51**, 12 (1987).
2) H. Tai, H. Tanaka, and T. Yoshino, Opt. Lett. **12**, 437 (1987).
3) M. D. DeGrandpre and L. W. Burgess, Anal. Chem. **60**, 2582 (1988).
4) B. D. Gupta, H. Dodeja, and A. K. Tomar, Opt. Quantum Electron. **28**, 1629 (1996).
5) P. Polynkin, A. Polynkin, N. Peyghambarian, and M. Mansuripur, Opt. Lett. **30**, 1273 (2005).
6) W. Liang, Y. Huang, Y. X. Reginald, K. Lee, and A. Yariv, Appl. Phys. Lett. **86**, 151122 (2005).
7) J. Villatoro and D. M. Hernandez, J. Lightwave Technol. **24**, 1409 (2006).
8) C. M. B. Cordeiro, M. A. R. Franco, G. Chesini, E. C. S. Barretto, R. Lwin, C. H. B. Cruz, and M. C. J. Large, Opt. Express **14**, 13056 (2006).
9) R. Jha, J. Villatoro, G. Badenes, and V. Pruneri, Opt. Lett. **34**, 617 (2009).
10) Y. Jung, S. Kim, D. Lee, and K. Oh, Meas. Sci. Technol. **17**, 1129 (2006).
11) Q. Wang and G. Farrell, Opt. Lett. **31**, 317 (2006).
12) S. Taue, Y. Matsumoto, H. Fukano, and K. Tsuruta, Jpn. J. Appl. Phys. **51**, 04DG14 (2012).
13) H. Fukano, Y. Matsumoto, and S. Taue, IEICE Electron. Express **9**, 302 (2012).
14) R. X. Gao, Q. Wang, F. Zhao, B. Meng, and S. L. Qu, Opt. Commun. **283**, 3149 (2010).
15) H. Fukano, Y. Kushida, and S. Taue, IEICE Electron. Express **10**, 20130812 (2013).
16) Y. Li, H. J. Schluesener, and S. Xu, Gold Bull. **43**, 29 (2010).
17) S. Underwood and P. Mulvaney, Langmuir **10**, 3427 (1994).
18) K. Mitsui, Y. Handa, and K. Kajikawa, Appl. Phys. Lett. **85**, 4231 (2004).
19) S. F. Cheng and L. K. Chau, Anal. Chem. **75**, 16 (2003).
20) M. Baia, F. Toderas, L. Baia, J. Popp, and S. Astilean, Chem. Phys. Lett. **422**, 127 (2006).
21) V. M. Shalaev, E. Y. Poliakov, and V. A. Markel, Phys. Rev. B **53**, 2437 (1996).
22) Y. T. Tseng, Y. J. Chuang, Y. C. Wu, C. S. Yang, M. C. Wang, and F. G. Tseng, Nanotechnology **19**, 345501 (2008).
23) S. Taue, H. Daito, and H. Fukano, Ext. Abstr. Int. Conf. Solid State Devices and Materials, 2014, p. 296.
24) L. B. Soldano and E. C. M. Pennings, J. Lightwave Technol. **13**, 615 (1995).
25) A. W. Snyder and J. D. Love, Appl. Opt. **15**, 236 (1976).
26) G. Frens, Nature **241**, 20 (1973).
27) S. Taue, K. Nishida, H. Sakaue, and T. Takahagi, e-J. Surf. Sci. Nanotechnol. **5**, 74 (2007).
28) M. Iga, A. Seki, and K. Watanabe, Sens. Actuators B **106**, 363 (2005).
29) G. Liu, Y. Wu, K. Li, P. Hao, and M. Xuan, Appl. Opt. **52**, 775 (2013).
30) T. A. Scott, Jr., J. Phys. Chem. **50**, 406 (1946).